

Zeeman splitting of 6.7 GHz methanol masers

On the uncertainty of magnetic field strength determinations^{*}

W. H. T. Vlemmings¹, R. M. Torres¹, and R. Dodson²

¹ Argelander Institute for Astronomy, University of Bonn, Auf dem Hügel 71, 53121 Bonn, Germany
e-mail: wouter@astro.uni-bonn.de

² International Centre for Radio Astronomy Research, University of Western Australia, Perth, Australia

Received 4 February 2011 / Accepted 4 March 2011

ABSTRACT

Context. To properly determine the role of magnetic fields during massive star formation, a statistically significant sample of field measurements probing different densities and regions around massive protostars needs to be established. However, relating Zeeman splitting measurements to magnetic field strengths needs a carefully determined splitting coefficient.

Aims. Polarization observations of, in particular, the very abundant 6.7 GHz methanol maser, indicate that these masers appear to be good probes of the large scale magnetic field around massive protostars at number densities up to $n_{\text{H}_2} \approx 10^9 \text{ cm}^{-3}$. We thus investigate the Zeeman splitting of the 6.7 GHz methanol maser transition.

Methods. We have observed of a sample of 46 bright northern hemisphere maser sources with the Effelsberg 100-m telescope and an additional 34 bright southern masers with the Parkes 64-m telescope in an attempt to measure their Zeeman splitting. We also revisit the previous calculation of the methanol Zeeman splitting coefficients and show that these were severely overestimated making the determination of magnetic field strengths highly uncertain.

Results. In total 44 of the northern masers were detected and significant splitting between the right- and left-circular polarization spectra is determined in >75% of the sources with a flux density $>20 \text{ Jy beam}^{-1}$. Assuming the splitting is due to a magnetic field according to the regular Zeeman effect, the average detected Zeeman splitting corrected for field geometry is $\sim 0.6 \text{ m s}^{-1}$. Using an estimate of the 6.7 GHz A-type methanol maser Zeeman splitting coefficient based on old laboratory measurements of 25 GHz E-type methanol transitions this corresponds to a magnetic field of $\sim 120 \text{ mG}$ in the methanol maser region. This is significantly higher than expected using the typically assumed relation between magnetic field and density ($B \propto n_{\text{H}_2}^{0.47}$) and potentially indicates the extrapolation of the available laboratory measurements is invalid. The stability of the right- and left-circular calibration of the Parkes observations was insufficient to determine the Zeeman splitting of the Southern sample. Spectra are presented for all sources in both samples.

Conclusions. There is no strong indication that the measured splitting between right- and left-circular polarization is due to non-Zeeman effects, although this cannot be ruled out until the Zeeman coefficient is properly determined. However, although the 6.7 GHz methanol masers are still excellent magnetic field morphology probes through linear polarization observations, previous derivations of magnetic fields strength turn out to be highly uncertain. A solution to this problem will require new laboratory measurements of the methanol Landé-factors.

Key words. masers – polarization – stars: formation – magnetic fields

1. Introduction

Maser observations have been able to provide important information on the magnetic field strength and structure in the densest areas of massive star forming regions and other astrophysical objects (for a review see e.g. Vlemmings 2007). As masers probe different densities and conditions, such as outflows, disks and shocks, combining the various maser observations can provide a detailed picture of the magnetic field that is needed for a proper understanding of these complex regions. The majority of the magnetic field information still comes from OH masers. These typically display a few mG field strength (e.g. Fish & Reid 2006; Bartkiewicz et al. 2005) and a coherent magnetic field structure. For example the polarization of the OH masers of W75N matches a toroidal field in a massive torus or disk (e.g. Hutawarakorn et al. 2002; Gray et al. 2003). The H₂O masers

mostly probe shock compressed fields and occasionally imply enhanced magnetic fields due to a nearby protostellar dynamo (e.g. Vlemmings et al. 2006a; Surcis et al. 2011). However, because of the shocked nature of the H₂O masers and the potential effect of Faraday rotation on the linear polarization of the OH masers, they are not necessarily the best probes of the magnetic field structure.

Recently, it has been discovered that methanol masers, one of the most numerous massive star formation maser species, also displays significant linear and circular polarization (e.g. Ellingsen 2002; Vlemmings et al. 2006b; Dodson 2008; Vlemmings 2008; Sarma & Momjian 2009). As methanol masers are less affected by Faraday rotation because of their higher frequency and as the different methanol maser transitions probe different areas of massive star formation, their potential in magnetic field studies is enormous. Unfortunately, the interpretation of maser polarization depends critically on the Zeeman frequency shift in relation to the maser saturation level

^{*} Table 2 and Figs. 5–7 are only available in electronic form at <http://www.aanda.org>

(e.g. [Watson 2009](#)) and determination of these quantities heavily relies on several assumptions. In this paper we present new observations of the splitting between the right- and left-polarization spectra of 6.7 GHz methanol masers to expand the sample presented in [Vlemmings \(2008, hereafter Paper I\)](#). We observed most of the strong northern- and southern-hemisphere 6.7 GHz masers, although splitting could only be detected in the northern sample because of calibration issues. While the splitting is attributed to the Zeeman effect, we show that an error was introduced in earlier Zeeman splitting calculations that makes the determination of magnetic field strength from the measured splitting highly uncertain.

2. Observations and analysis

2.1. Effelsberg observations

The observations of the northern maser sample were taken on June 17–19th and June 27th 2008 using the 5 cm primary focus receiver of the 100-m Effelsberg¹ telescope. The full width at half-maximum (*FWHM*) beam of the telescope is ~ 2 arcmin at the maser frequency. The setup was identical to that used in Paper I. We used a position-switch mode with a 2 min cycle time and the data were collected using the fast Fourier transform spectrometer (FFTS) with two spectral windows, corresponding to the right- and left-circular polarizations (RCP and LCP). The spectral windows of 20 MHz were divided in 16 384 spectral channels, resulting in a ~ 0.055 km s⁻¹ channel spacing and were centered on the local standard of rest (LSR) source velocities.

The data were reduced using the Continuum and Line Analysis Single-dish Software (CLASS) package and the amplitudes were calibrated using scans on 3C 286. As some of the data was taken with the same setup and at the same date of the monitoring observations of G9.62+0.20 ([Vlemmings et al. 2009, hereafter V09](#)), we were able to compare the fluxes with simultaneous Hartebeesthoek radio telescope observations of that source (Goedhart, priv. comm.). From this we estimate the absolute flux errors to be $\sim 10\%$. Any larger flux variations are likely due to maser variability and/or intrinsic changes of the maser structure.

2.2. Parkes observations

The southern maser sample was observed with the Parkes 64-m telescope using the methanol multibeam (MMB) receiver between Aug. 15–18th 2008. The MMB system is detailed in [Green et al. \(2009\)](#). Only two beams of the receiver were used, performing beam switching with a 2 min cycle time. We observed two windows, centered on the LSR source velocity for the 6.7 GHz methanol maser transition and for the 6.035 GHz excited OH maser transition respectively. The OH maser observations will be presented in a forthcoming paper (Torres et al., in prep.). The *FWHM* of the Parkes beam at 6.7 GHz is 3.2 arcmin. Using the spectrometer with 2048 channels and a bandwidth of 4 MHz, we reach a spectral resolution of ~ 0.09 km s⁻¹.

The data calibration was performed using the single-dish ATNF Spectral Analysis Package (ASAP) embedded in the Common Astronomy Software Applications (CASA) package. Unfortunately, the scan-to-scan stability of the RCP- and LCP-signals turned out to be insufficient to determine the Zeeman

splitting. Although the exact cause of this is unclear, the most likely explanation is a lack of baseline stability on short time scales and potential narrow baseline ripples that cannot be removed by a low polynomial baseline fit. Thus, the further analysis in the paper is focused on the Effelsberg observations. For completeness, the total intensity maser spectra and derived peak and integrated fluxes are presented in the online material, Fig. 7, and Table 2.

2.3. Source selection

The Effelsberg sample was taken from the 6.7 GHz methanol maser catalogue by [Pestalozzi et al. \(2005\)](#) and consists of the strongest (>50 Jy) northern maser sources observable from Effelsberg. The first part of the sample was presented in Paper I but is also presented here for completeness. As a number of the masers display significant difference in the catalogue flux and the observed flux, several of the sources presented here fall below the 50 Jy limit imposed during source selection. The Parkes sample was taken from the same catalogue but limited to the Southern sources with a listed flux >100 Jy. To detect the Zeeman splitting the goal was to reach a signal-to-noise of >3000 and thus the total integration time per source was variable. When an initial scan indicated the observed flux was significantly lower than the catalog flux and as a result a Zeeman splitting detection would be unlikely within reasonable time, integration time was typically shortened. Thus, the noise level varies from source to source and ranges from 20 mJy to 100 mJy for each polarization.

2.4. Analysis method

As in Paper I and V09, we used the cross-correlation between the RCP and LCP signals to determine the Zeeman splitting of the methanol masers. The advantage of this method is, that it is insensitive to relative gain calibration errors between the two polarization. In the case of methanol Zeeman splitting this is specifically important, as the splitting is typically of order 0.5 m s⁻¹. The circular polarization arising from such small splitting is $<0.5\%$ (Paper I).

2.5. Error analysis

The errors on the Zeeman splitting determination depend on the rms noise in the RCP and LCP maser spectra. However, it was shown in V09, that for masers stronger than 50 Jy beam⁻¹, the noise in the channels with maser emission increases. We have thus corrected the Zeeman splitting values determined in Paper I following the relation found in V09 between rms channel noise and maser flux. Note that the error estimates are thus very conservative, as we have taken the rms noise in the channel with the strongest maser emission to determine the total Zeeman splitting error.

3. Methanol maser Zeeman splitting

3.1. Uncertainty in the splitting coefficient

The methanol molecule is a non-paramagnetic molecule and as a result the Zeeman splitting under the influence of a magnetic field is extremely small. The split energy, ΔE_z , of an energy level under the influence of a magnetic field, B , can be described as $\Delta E_z = g_L \mu_N M_J B$, where M_J denotes the magnetic quantum

¹ The 100-m telescope at Effelsberg is operated by the Max-Planck-Institut für Radioastronomie (MPIfR) on behalf of the Max-Planck-Gesellschaft (MPG).

number for the rotational transition described with the total angular momentum quantum number J , B is the magnetic field strength in units of Tesla ($=10^4$ G), μ_N is the nuclear magneton and g_L is the Landé g -factor. The Zeeman effect is determined by the Landé g -factor, which needs to be determined from laboratory spectroscopy.

In the previous publications of methanol polarization, the g -factor used to determine the magnetic field strength was based on laboratory measurements performed many years ago on a number of methanol transitions near 25 GHz methanol (Jen 1951). He found empirically that the methanol g -factor, could be described by the equation:

$$g_L = 0.078 + 1.88/[J(J+1)]. \quad (1)$$

However, there are several caveats regarding these measurements. Firstly, g_L is an average of the true g -factor of several interacting states. Additionally, the measurements are classified as preliminary in Jen (1951), and the exact transitions that were used are not specified. The observations were done on poorly identified transitions around 25 GHz with $\Delta J = 0$ and $K = 2-1$, which likely indicates it concerns the E1-type methanol maser. It is thus not impossible that an extrapolation to the 6.7 GHz 5_1-6_0 A⁺ methanol transition and others transitions with different ΔJ and quantum number K is invalid.

While it is thus unclear if the g -factor determined in 1951 can be used for the 6.7 GHz methanol maser, it is the only estimate available to us at the moment. Using this, Vlemmings et al. (2006b) determined the Zeeman splitting coefficient to be $0.049 \text{ km s}^{-1} \text{ G}^{-1}$. After a reanalysis, it was recently found that an unfortunate calculation error was introduced in that paper. The actual Zeeman splitting coefficient for the 5_1-6_0 A⁺ 6.7 GHz methanol maser transition extrapolated from the laboratory measurements is $0.005 \text{ km s}^{-1} \text{ G}^{-1}$, an order of magnitude smaller than previously determined. This error has also affected the magnetic field calculations of the other methanol maser transitions (e.g. Sarma & Momjian 2009).

If we can still attribute the measured splitting between the RCP- and LCP-spectra of the 6.7 GHz methanol maser as standard Zeeman splitting, the implication of the new Zeeman splitting coefficient is that the magnetic field strength in the methanol maser region is an order of magnitude larger. Based on the results in Paper I, this would thus imply that the magnetic field is of order 100 mG. In that case, the magnetic field measured on the methanol masers is almost two orders of magnitude stronger than that measured on OH masers (e.g. Fish & Reid 2006). Considering the empirically determined scaling relation $B \propto n_{\text{H}_2}^{0.47}$ (Crutcher 1999) and the indication that the methanol masers exist in gas with a density at most an order of magnitude larger than that of the OH masers (e.g. Green et al. 2007), such a large difference between the methanol and OH determined magnetic field strength is surprising. This seems to imply that the extrapolated g -factor is uncertain by an order of magnitude or potentially that instrumental or other non-Zeeman effects dominate the 6.7 GHz splitting measurements.

3.2. Potential non-Zeeman effects

As the best estimate for the 6.7 GHz Zeeman coefficient is much smaller than previously assumed, the determined magnetic fields based on the regular Zeeman effect are much larger than would be expected. We thus need to again determine if non-Zeeman effects could be the cause of the observed splitting between the RCP- and LCP-signal.

First we need to consider instrumental effects. The 6.7 GHz methanol maser splitting was first measured with the 100-m Effelsberg telescope (Paper I). In our monitoring observations (V09), we have shown the observed splitting to be reproducible and the observing system to be robust. The splitting of the masers in W75N was later confirmed in high-angular resolution European VLBI Network (EVN) observations (Surcis et al. 2009). Additionally, recent observations with the Hobart 26-m antenna confirmed the splitting of G09.62+0.20 (Ellingsen, priv. comm.). Therefore instrumental effects can likely be ruled out.

Another effect is the propagation of strong linear polarization that can cause circular polarization when the direction of the magnetic field changes significantly along the maser propagation direction (Wiebe & Watson 1998). For a smooth change of magnetic field direction of ~ 1 rad along the maser, the fractional circular polarization caused by this effect is approximately $m_l^2/4$, where m_l is the fractional linear polarization. The typical polarization observed in high angular resolution observations is 1–4% (e.g. Vlemmings et al. 2006b; Dodson 2008; Surcis et al. 2009), indicating that this effect contributed at most $\sim 0.04\%$, a fraction of the observed values.

Finally, a potentially important effect is caused by a rotation of the axis of symmetry for the molecular quantum states. This can occur when, as the maser brightness increases while it becomes more saturated, the rate for maser stimulated emission R becomes larger than the Zeeman frequency shift $g\Omega$. While $g\Omega \gg R$, the magnetic field direction is the quantization axis. Then, when R becomes larger than $g\Omega$, the molecules interact more strongly with the radiation field than with the magnetic field and the quantization axis changes towards the maser propagation direction. This change will cause an intensity-dependent circular polarization that mimics the regular Zeeman splitting. This has been shown by Nedoluha & Watson (1990a) for a $J = 2-1$ transition although the effect decreases for transitions with higher angular momentum such as the 6.7 GHz methanol maser and the exact magnitude is hard to determine.

From the recalculated Zeeman splitting coefficient derived above, $g\Omega \approx 0.1B[\text{mG}] \text{ s}^{-1}$ for the 6.7 GHz methanol maser. The rate for stimulated emission can be estimated using:

$$R \approx AkT_b\Delta\Omega/4\pi h\nu. \quad (2)$$

Here A is the Einstein coefficient for the maser transition, which is equal to $0.1532 \times 10^{-8} \text{ s}^{-1}$ (Cragg et al. 1993), and k and h are the Boltzmann and Planck constants respectively. The maser frequency is denoted by ν , and T_b and $\Delta\Omega$ are the maser brightness temperature and beaming solid angle. The ratio between zeeman splitting and rate of stimulated emission for the 6.7 GHz methanol masers, assuming the recalculated g -factor, can thus be given by:

$$g\Omega/R \approx 13 \frac{[B]}{[5 \text{ mG}]} \frac{[10^{10} \text{ K}]}{[T_b]} \frac{[10^{-2} \text{ sr}]}{[\Delta\Omega]}. \quad (3)$$

Our observations indicate typically $T_b \lesssim 10^{10} \text{ K}$ (Surcis et al. 2009; Vlemmings et al. 2010), although for the brightest masers $T_b \sim 10^{12}$ (Minier et al. 2002). The beaming angle $\Delta\Omega$ is harder to estimate and decreases rapidly with increasing maser saturation level. For H₂O masers, beaming angles have been estimated to be of order 10^{-5} – 10^{-4} (Nedoluha & Watson 1991). If we very conservatively assume a maser beaming angle of $\Delta\Omega \approx 10^{-2}$, the typical maser stimulated emission $R \sim 0.04 \text{ s}^{-1}$, and for the most saturated masers $R \lesssim 4 \text{ s}^{-1}$, even without considering the rapid decrease of $\Delta\Omega$ due to the fact that beaming becomes much more pronounced for the stronger masers. Thus, typically, $g\Omega/R > 1$

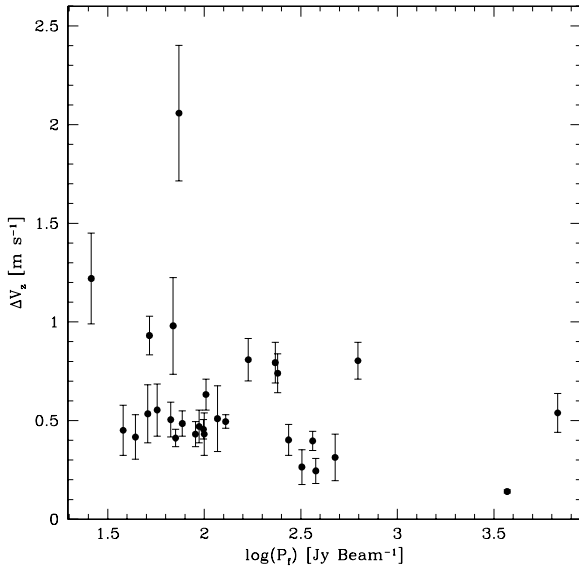


Fig. 1. Observed splitting between the right- and left-polarization spectra vs. the maser peak flux. The lack of an increase of the splitting with flux argues against a non-Zeeman interpretation of the observed splitting.

and only for the most saturated masers would we expect the non-Zeeman effect to be applicable. As detailed in V09, this could be the cause for the circular polarization variability seen during the flare of G09.62+0.20. Another indication that non-Zeeman effects are not the cause of the observed splitting is the lack of an observed relation between maser flux and the RCP- and LCP-splitting illustrated in Fig. 1. Even ignoring the strongest masers, W3OH and G09.62+0.20, due to their complicated maser structure and flaring nature respectively, it is clear that the observed splitting is independent of maser flux.

Thus, there are no indications of a non-Zeeman contribution to the observed splitting, which we consequently still attribute to actual Zeeman splitting. However, the exact Zeeman splitting coefficient is highly uncertain and we cannot determine the exact field strength. Based on the measurements of W75N, where, assuming a splitting coefficient of $0.049 \text{ km s}^{-1} \text{ G}^{-1}$, the methanol maser magnetic field is identical to the field measured during an OH maser flare (Surcis et al. 2009), we suggest that the originally assumed Zeeman splitting coefficient is closer to the actual value. New laboratory measurements are needed to settle this issue. Thus, the derived magnetic field strengths could be different by an order of magnitude. However, with the non-Zeeman effect unlikely to be in effect, linear polarization measurements still are excellent probes of the magnetic field morphology, especially as the linear polarization fraction appears to be too low to be due to anisotropic pumping even for such small $g\Omega$ (Nedoluha & Watson 1990b). Additionally, as g_L is a signed quantity, with its sign not in doubt, the Zeeman splitting measurements still reveal the direction of the magnetic field, with negative Zeeman splitting values indicating a field oriented towards the observer.

4. Results

4.1. Zeeman splitting

The results of our survey are presented in Table 1. The table lists the source name, possible alternate names, the central V_{LSR} velocity, peak and integrated fluxes and the measured Zeeman

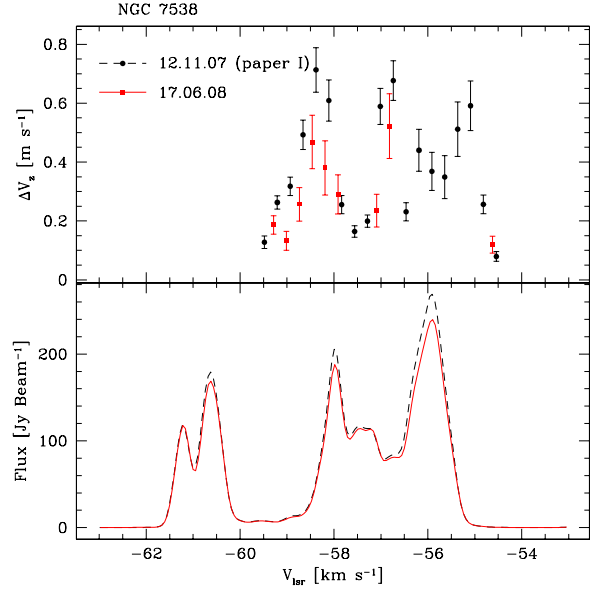


Fig. 2. Total intensity spectrum (*bottom*) and Zeeman splitting (*top*) for G111.43+076 (NGC 7538). The red solid line and square symbols denote the measurements presented in Paper I, taken at Nov. 12th 2007, the black dashed line and solid circles are the measurements presented here.

splitting ΔV_z . This value of the splitting corresponds to the flux averaged Zeeman splitting of the entire maser spectrum and can be used to determine the line-of-sight magnetic field strength (B_{\parallel}) using the Zeeman coefficient of $0.005 \text{ m s}^{-1} \text{ G}^{-1}$. As described in Sect. 3 however, this Zeeman coefficient value is highly uncertain and is potentially wrong by an order of magnitude. The table lists the sources from Paper I with the increased error bars. For the sources with significant changes of the Zeeman splitting between different spectral features, we list multiple values. Total intensity spectra and Zeeman splitting determined across the spectrum are presented in online Fig. 5. The total intensity spectra of the sources with no Zeeman splitting detection are shown in online Fig. 6. The sources observed with the Parkes telescope are listed with V_{LSR} velocity and peak and integrated fluxes in online Table 2. The spectra are shown in online Fig. 7.

4.2. Comparison between observing epochs

Although the stability of the Effelsberg polarization measurements was already confirmed by the monitoring observations of G09.62+0.20 presented in V09, we performed additional tests, observing 5 sources that were previously observed in Paper I. This included three sources for which we had only determined an upper limit to the Zeeman splitting. As can be seen in Table 1, the flux averaged Zeeman splitting of both G12.89-0.49 (IRAS 18089-1732) and G111.53+0.76 (NGC 7538) are fully consistent at the two epochs. As shown in Fig. 2, also the variation of Zeeman splitting across the maser spectrum of G111.53+0.76 is reproduced. The only difference is the non-detection of the field around -56 km s^{-1} , which is due to the fact that we spent slightly less observing time on this source in the second epoch and thus cannot confirm the earlier detection, that was close to 3σ , in this velocity interval. In the observations presented here, we were able to determine the Zeeman

Table 1. Zeeman splitting results.

Source		α_{J2000} hh mm ss	δ_{J2000} ° ' "	V_{LSR} km s ⁻¹	Peak flux Jy beam ⁻¹	Int. flux Jy beam ⁻¹ km s ⁻¹	ΔV_z^a m s ⁻¹
G10.32-0.15	IRAS 18060-2005	18 09 01.46	-20 05 08.00	10.0	100	152	0.43 ± 0.11
G10.47+0.02 ^b	IRAS 18056-1952	18 08 38.21	-19 51 49.50	75.0	38	96	0.45 ± 0.13
G11.49-1.48 ^b	IRAS 18134-1942	18 16 22.13	-19 41 27.50	6.2	77	176	0.48 ± 0.07
G12.02-0.03	IRAS 18090-1832	18 12 01.85	-18 31 55.50	108.0	102	118	0.63 ± 0.08
G12.68-0.18 ^b	W33B	18 13 54.20	-18 01 44.00	52.0	378	996	0.24 ± 0.06
G12.71-0.11		18 13 43.40	-17 58 06.00	57.7	–	–	–
G12.89+0.49 ^c	IRAS 18089-1732	18 11 51.46	-17 31 28.84	39.0	57	75	0.55 ± 0.13
G14.09+0.10	IRAS 18128-1640	18 15 41.70	-16 38 57.00	15.1	51	84	<0.44
G18.34+1.78	IRAS 18151-1208	18 17 54.10	-12 06 48.00	27.7	44	23	0.42 ± 0.11
G20.24+0.07	IRAS 18249-1116	18 27 44.56	-11 14 54.60	71.4	23	21	<0.76
G23.44-0.18 ^b	IRAS 18319-0834	18 34 39.27	-08 31 39.00	103.0	90	178	0.43 ± 0.06
G24.78+0.08	W42	18 36 12.57	-07 12 11.50	113.0	129	188	0.50 ± 0.03
G25.65+1.04	IRAS 18316-0602	18 34 20.91	-05 59 40.50	41.9	99	43	0.46 ± 0.05
G25.71+0.04 ^c	IRAS 18353-0628	18 38 03.15	-06 24 15.00	95.6	625	620	0.81 ± 0.10
G28.82+0.48		18 42 12.43	-03 25 39.50	83.3	1.6	3.1	<7.5
G29.86-0.04 ^b		18 45 59.53	-02 44 47.00	101.4	67	87	0.50 ± 0.08
				104.0			-0.67 ± 0.17
G29.95-0.02	W43S	18 46 03.74	-02 39 21.43	96.0	169	227	-0.33 ± 0.11
G30.91+0.14		18 47 15.00	-01 44 07.00	104.0	12	28	<4.0
G32.03+0.06 ^{b,c}	IRAS 18470-0050	18 49 37.30	-00 45 47.00	98.7	117	165	0.51 ± 0.17
				101.0			-0.22 ± 0.06
G33.68-0.26	IRAS 18512+0029	18 53 45.20	00 32 47.00	62.6	–	–	–
G35.02+0.35	IRAS 18515+0157	18 54 00.60	02 00 50.00	44.0	26	29	1.22 ± 0.23
G41.34-0.14	IRAS 19049+0720	19 07 21.87	07 25 17.34	12.0	18	27	<3.8
G43.80-0.13 ^{b,c}	W49N	19 11 55.10	09 36 00.00	40.0	40	38	<0.31
				43.0			1.36 ± 0.33
G49.57-0.38	IRAS 19216+1429	19 23 53.60	14 34 54.00	59.3	2.6	2.4	<4.92
G108.18+5.51	IRAS 22272+6358	22 28 52.00	64 13 22.00	-10.9	51	34	0.53 ± 0.15
G111.53+0.76 ^c	NGC 7538	23 13 45.36	61 28 10.55	-56.2	240	552	0.74 ± 0.10
G196.45-1.69	S269	06 14 37.06	13 49 37.00	15.0	18	14	<0.77
Previous observations (Paper I)							
G09.62+0.20 ^b		18 06 14.66	-20 31 31.57	1.0	6757	3091	0.54 ± 0.10
G12.89+0.49 ^{b,c}	IRAS 18089-1732	18 11 51.46	-17 31 28.84	39.0	71	105	0.41 ± 0.04
G23.01-0.41 ^b		18 34 40.37	-09 00 38.30	74.8	585	1016	-1.49 ± 0.21
G25.71+0.04 ^c		18 38 03.15	-06 24 15.00	95.6	590	591	<0.56
G25.83-0.18		18 39 04.70	-06 24 17.00	90.7	69	84	0.99 ± 0.26
G28.15+0.00		18 42 41.00	-04 15 21.00	101.3	30	24	<1.8
G31.28+0.06	IRAS 18456-0129	18 48 12.38	-01 26 22.60	110.4	74	174	2.06 ± 0.36
G32.03+0.06 ^c	IRAS 18470-0050	18 49 37.30	-00 45 47.00	98.7	69	81	<1.0
G33.64-0.21		18 53 28.70	00 31 58.00	58.6	63	54	-0.89 ± 0.20
G35.20-0.74	IRAS 18556+0136	18 58 12.98	01 40 37.50	30.5	169	167	0.81 ± 0.11
G35.20-1.74	W48	19 01 45.60	01 13 28.00	41.5	476	643	0.32 ± 0.12
G37.40+1.52	IRAS 18517+0437	18 54 13.80	04 41 32.00	41.0	320	193	0.75 ± 0.09
G43.80-0.13 ^c	W49N	19 11 55.10	09 36 00.00	40.0	35	81	<1.9
G49.49-0.39	W51-e1/e2	19 23 44.50	14 30 31.00	59.0	1029	885	<1.2
G69.52-0.97	ON1	20 10 09.07	31 31 34.40	11.6	96	45	<0.34
G78.10+3.64	IRAS 20126+4104	20 14 26.04	41 13 33.39	-6.1	60	77	<0.93
G81.87+0.78 ^b	W75N	20 38 36.42	42 37 34.85	5.0	273	317	0.40 ± 0.08
G109.86+2.10	Cepheus A	22 56 18.09	62 01 49.45	-4.2	364	484	0.39 ± 0.05
G111.53+0.76 ^{b,c}	NGC 7538	23 13 45.36	61 28 10.55	-56.2	233	514	0.79 ± 0.10
G133.94+1.04	W3(OH)	02 27 03.77	61 52 24.55	-44.0	3705	8198	0.141 ± 0.009
G173.49+2.42	S231	05 39 13.06	35 45 51.29	-13.0	52	53	0.95 ± 0.11
G174.19-0.09	AFGL 5142	05 30 42.00	33 47 14.00	2.1	55	34	<0.8
G188.95+0.89	IRAS 06058+2138	06 08 53.35	21 38 28.67	10.9	633	485	-0.49 ± 0.15
G192.60-0.05	S255	06 12 54.02	17 59 23.00	5.0	94	78	0.47 ± 0.08

Notes. ^(a) B_{\parallel} can be derived by dividing ΔV_z by the Zeeman splitting coefficient appropriate for the 6.7 GHz transition of methanol, see Sect. 3.

^(b) Significant magnetic field changes across the maser spectrum. ^(c) Observed both epochs.

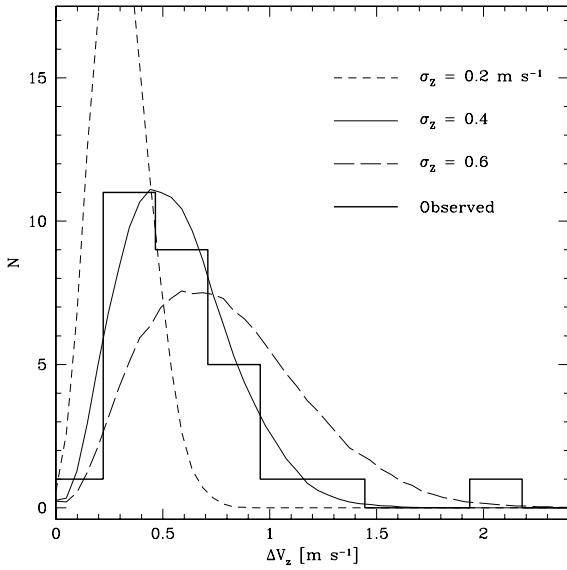


Fig. 3. Distribution of observed Zeeman splitting (thick solid line) in the Effelsberg 6.7 GHz methanol maser sample. Over-plotted are models for the line of sight Zeeman splitting in the case of where the magnetic field is taken to have a Gaussian distribution with a Zeeman splitting dispersion of σ_Z in each dimension. Following a simple analysis, the best fitted model has $\sigma_Z = 0.4 \text{ m s}^{-1}$ which would correspond to a full 3-dimensional equivalent Zeeman splitting of $\langle \Delta V_z \rangle \approx 0.62 \text{ m s}^{-1}$. As an indication, using the uncertain laboratory extrapolated g -factor (Sect. 3) this corresponds to $\langle |B| \rangle \approx 120 \text{ mG}$.

splitting on the other three sources (G25.71+0.04, G32.03+0.06 and G43.80-0.13) by increasing the observing time. These values were in agreement with the previously determined upper limits for G32.03+0.06 and G43.80-0.13, while for G25.71+0.04 the current value should have been detected at the 4σ level. As the other sources indicate good stability, we thus conclude that for this specific source a small intrinsic change has occurred in the flux averaged field strength.

5. Discussion

Although we attribute the observed splitting between the RCP- and LCP-spectra as true Zeeman splitting we cannot derive a meaningful magnetic field strength. We plot the distribution of measured Zeeman splitting in Fig. 3. To obtain an indication of the total magnetic field, we assume the field to have a random orientation with each one dimensional field component described by a Gaussian distribution with dispersion σ_Z . We then perform Monte-Carlo modeling of the observed Zeeman splitting distribution using a description of the detection limit that describes the error bars of our observations. Three of these distributions are also shown in Fig. 3. We do not perform any further statistical tests, as the Zeeman coefficient uncertainty will dominate any final results and the described magnetic field model is unlikely to be realistic, but the best fit to the observed distribution is found for $\sigma_Z \approx 0.4 \text{ m s}^{-1}$. If the laboratory value can be extrapolated to the 6.7 GHz methanol masers this would indicate a rather high average field strength of $\langle |B| \rangle \approx 120 \text{ mG}$. For comparison, the typical field strength measured in OH masers $|B_{\text{OH}}| \approx 5$ (Fish & Reid 2006). If methanol masers exist in gas with H_2 number densities of order 10^8 cm^{-3} (Cragg et al. 2005), at most an order of magnitude more than the typical density of

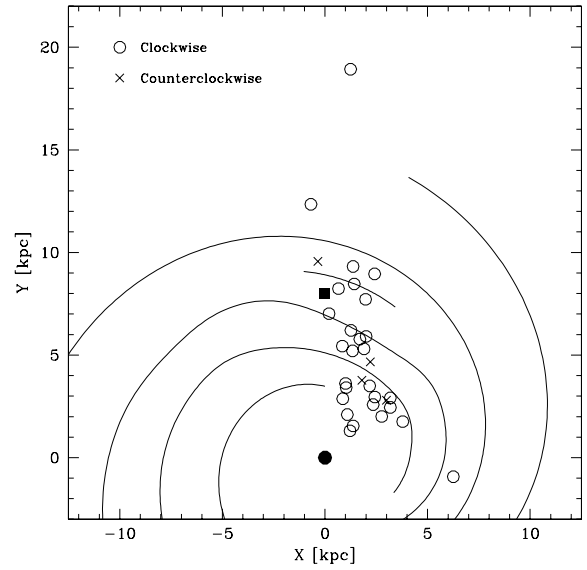


Fig. 4. Magnetic field direction derived from the methanol maser Zeeman splitting observations presented in this paper projected onto the Galactic plane. The symbols are the observed star forming region with kinematic distances from Pestalozzi et al. (2005) unless better distances were available. The open circles and crosses indicate a clockwise and counterclockwise magnetic field direction respectively. The approximate location of the spiral arms is indicated as taken from Taylor & Cordes (1993).

OH masers, the magnetic field vs. density relation from Crutcher (1999) ($B \propto n^{0.47}$) would predict an average methanol field strength $|B_{\text{meth}}| \approx 15 \text{ mG}$. This would be consistent with the values derived from the Zeeman splitting only if the Zeeman splitting coefficient for the 6.7 GHz A-type methanol is an order of magnitude larger than the value extrapolated from the 25 GHz E-type methanol Landé-factor measurements.

Despite the uncertainty in the magnitude of the Landé factor, the sign of Zeeman splitting is not in question. The observations thus represent a large set of line-of-sight magnetic field directions toward massive star forming regions. It has been suggested that the magnetic field direction measured in interstellar OH masers might be linked to the overall Galactic magnetic field (Davies 1974). As we have previously shown in Paper I that the sign of the methanol maser derived magnetic field direction corresponds well with that derived from OH masers, as similar link might thus exist between the field direction determined from methanol masers and the Galactic magnetic field. In Fig. 4 we show the magnetic field direction measured for our complete sample projected onto the Galactic plane. The observations show that the vast majority of the masers display a clockwise oriented magnetic field consistent with Galactic rotation. However, one would have to question if the densest regions of star formation retain a magnetic field aligned with the Galactic field through compression and likely rotation. A more thorough analysis of OH maser Zeeman splitting results does not support such a relation (Fish et al. 2003), and also more recent work based on dust linear polarization observations find no clear relation between the large scale Galactic magnetic field structure and that measured in star forming regions (Stephens et al. 2011). Still, the clear preference for a clockwise field orientation in the methanol maser regions is suggestive of a global trend. A more detailed analysis is however beyond the scope of this paper.

6. Concluding remarks

This paper presents Zeeman splitting measurements obtained on a flux limited sample of 6.7 GHz methanol masers. The observations of this unique tracer of massive star formation were performed with the Effelsberg and Parkes radio-telescopes. Unfortunately, the stability of the Parkes observations precluded the determination of Zeeman splitting and our sample is thus limited to sources observable from Effelsberg. The 6.7 GHz methanol masers are good tracers of the large scale structure of the magnetic field in the massive star formation regions at densities of $n_{\text{H}_2} \approx 10^8 \text{ cm}^{-3}$. However, here we have shown that previous magnetic field strength determinations were in error and that the exact Zeeman splitting coefficient is extremely uncertain. Assuming a calculation of the 6.7 GHz A-type methanol transition Landé g -factor extrapolated from laboratory measurements for an average of E-type methanol 25 GHz transitions, the geometry corrected total magnetic field in the methanol maser region $\langle |B| \rangle = 120 \text{ mG}$. This is an order of magnitude higher than expected and likely indicates the g -factor cannot simply be extrapolated. Still, instrumental effect or non-Zeeman interpretations of the observed splitting are unlikely as no relation between maser flux and splitting is observed and as the observations are reproduced with a number of different telescopes and for different methanol maser transitions. The Zeeman splitting uncertainty has been shown to have little effect on the linear polarization measurements presented in other papers, but the field determination accuracy will only improve with new laboratory measurements of the correct g -factors. Still, we have detected significant Zeeman splitting in 76% of the sources with peak fluxes down to $\sim 20 \text{ Jy}$, which, unless the true g -factor is much more than an order of magnitude wrong, suggests relatively strong magnetic fields are widespread.

Acknowledgements. W.V. thanks Alex Kraus for his help setting up the Effelsberg observations. W.V. also thanks Vladimir Strelitski for pointing out the calculation error in the previous publications and Simon Ellingsen for communicating the results of his Hobart telescope Zeeman splitting confirmation. We further acknowledge useful discussion with Anuj Sarma and Vincent Fish.

This research was supported by the Deutsche Forschungsgemeinschaft (DFG) through the Emmy Noether Research grant VL 61/3-1.

References

- Bartkiewicz, A., Szymczak, M., Cohen, R. J., & Richards, A. M. S. 2005, *MNRAS*, 361, 623
- Cragg, D. M., Mikhtiev M. A., Bettens, R. P. A., et al. 1993, *MNRAS*, 264, 769
- Cragg, D. M., Sobolev, A. M., & Godfrey, P. D. 2005, *MNRAS*, 360, 533
- Crutcher, R. M. 1999, *ApJ*, 520, 706
- Davies, R. D. 1974, in *Galactic Radio Astronomy*, ed. F. J. Kerr, & S. C. Simonson III (Dordrecht: Reidel), IAU Symp., 60, 275
- Dodson, R. 2008, *A&A*, 480, 767
- Ellingsen, S. P. 2002, in *Cosmic Masers: From Proto-Stars to Black Holes*, ed. V. Migenes, & M. J. Reid, IAU Symp., 206, 151
- Fish, V. L. & Reid, M. J. 2006, *ApJS*, 164, 99
- Fish, V. L., Reid, M. J., Argon, A. L., & Menten, K. M. 2003, *ApJ*, 596, 328
- Gray, M. D., Hutawarakorn, B., & Cohen, R. J. 2003, *MNRAS*, 343, 1067
- Green, J. A., Richards, A. M. S., Vlemmings, W. H. T., Diamond, P., & Cohen, R. J. 2007, *MNRAS*, 382, 770
- Green, J. A., Caswell, J. L., Fuller, G. A., et al. 2009, *MNRAS*, 392, 783
- Hutawarakorn, B., Cohen, R. J., & Brebner, G. C. 2002, *MNRAS*, 330, 349
- Jen, C. K. 1951, *Phys. Rev.*, 81, 197
- Minier, V., Booth, R. S., & Conway, J. E. 2002, *A&A*, 383, 614
- Nedoluha, G. E., & Watson, W. D. 1990a, *ApJ*, 354, 660
- Nedoluha, G. E., & Watson, W. D. 1990b, *ApJ*, 361, L53
- Nedoluha, G. E., & Watson, W. D. 1991, *ApJ*, 367, L63
- Pestalozzi, M. R., Minier, V., & Booth, R. S. 2005, *A&A*, 432, 737
- Sarma, A. P., & Momjian, E. 2009, *ApJ*, 705, L176
- Stephens, I. W., Looney, L. W., Dowell, C. D., Vaillancourt, J. E., & Tassis, K. 2011, *ApJ*, 728, 99
- Surcis, G., Vlemmings, W. H. T., Dodson, R., & van Langevelde, H. J. 2009, *A&A*, 506, 757
- Surcis, G., Vlemmings, W. H. T., Curiel, S., et al. 2011, *A&A*, 527, 48
- Taylor, J. H., & Cordes, J. M. 1993, *ApJ*, 411, 674
- Vlemmings, W. H. T. 2007, IAU Symp., 242, 37
- Vlemmings, W. H. T. 2008, *A&A*, 484, 773 (Paper I)
- Vlemmings, W. H. T., Diamond, P. J., van Langevelde, H. J., & Torrelles, J. M. 2006a, *A&A*, 448, 597
- Vlemmings, W. H. T., Harvey-Smith, L., & Cohen, R. J. 2006b, *MNRAS*, 371, L26
- Vlemmings, W. H. T., Goedhart, S., & Gaylard, M. J. 2009, *A&A*, 500, L9 (V09)
- Vlemmings, W. H. T., Surcis, G., Torstensson, K. J. E., & van Langevelde, H. J. 2010, *MNRAS*, 404, 134
- Watson, W. D. 2009, *Rev. Mex. Astron. Astrofis. Conf. Ser.*, 36, 113
- Wiebe, D. S., & Watson, W. D. 1998, *ApJ*, 503, L71

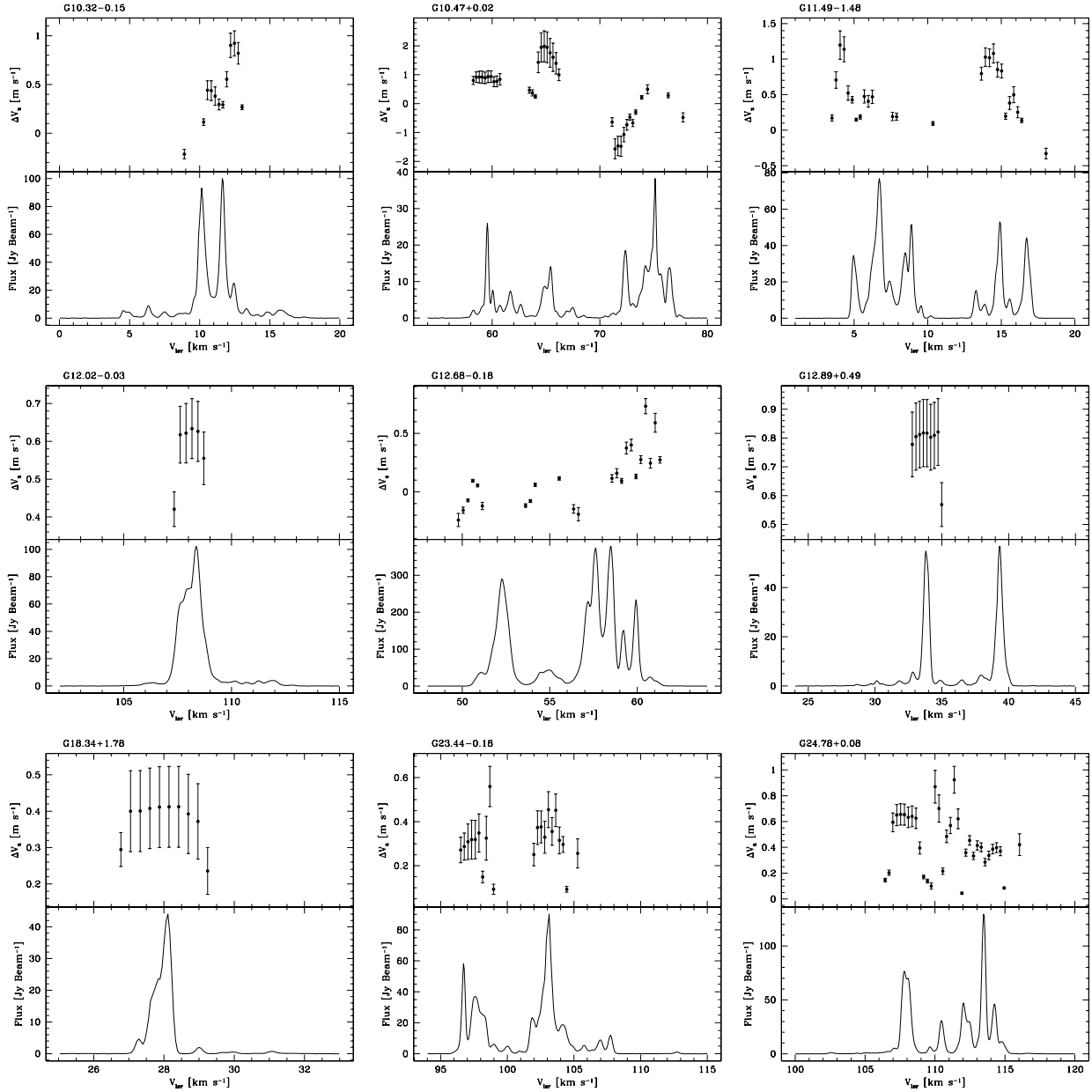


Fig. 5. Total intensity spectra (*bottom*) and Zeeman splitting (*top*) for all the sources of our sample with a significant detection. The Zeeman splitting is derived using the “running” cross-correlation method (see Paper I).

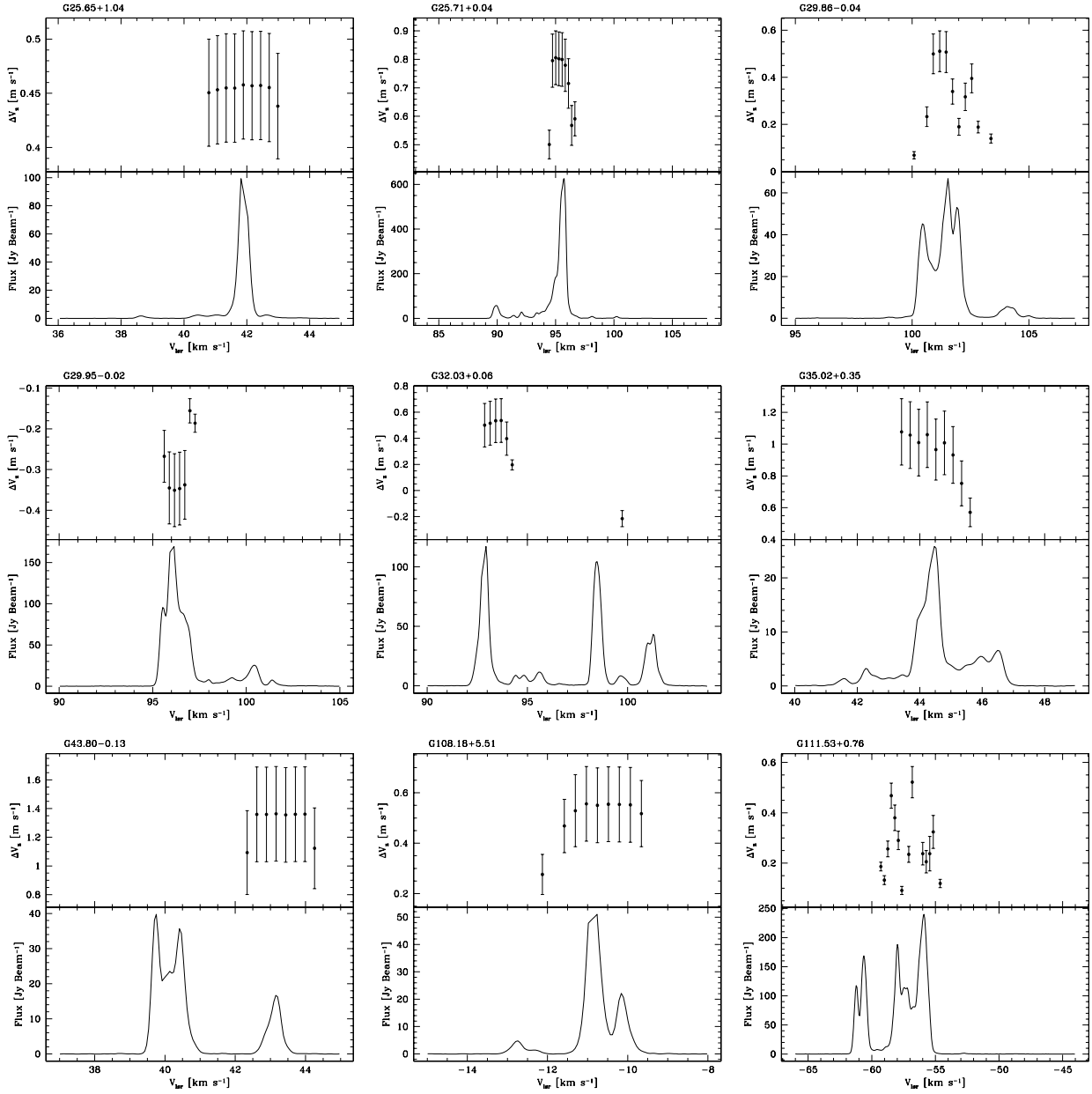


Fig. 5. continued.

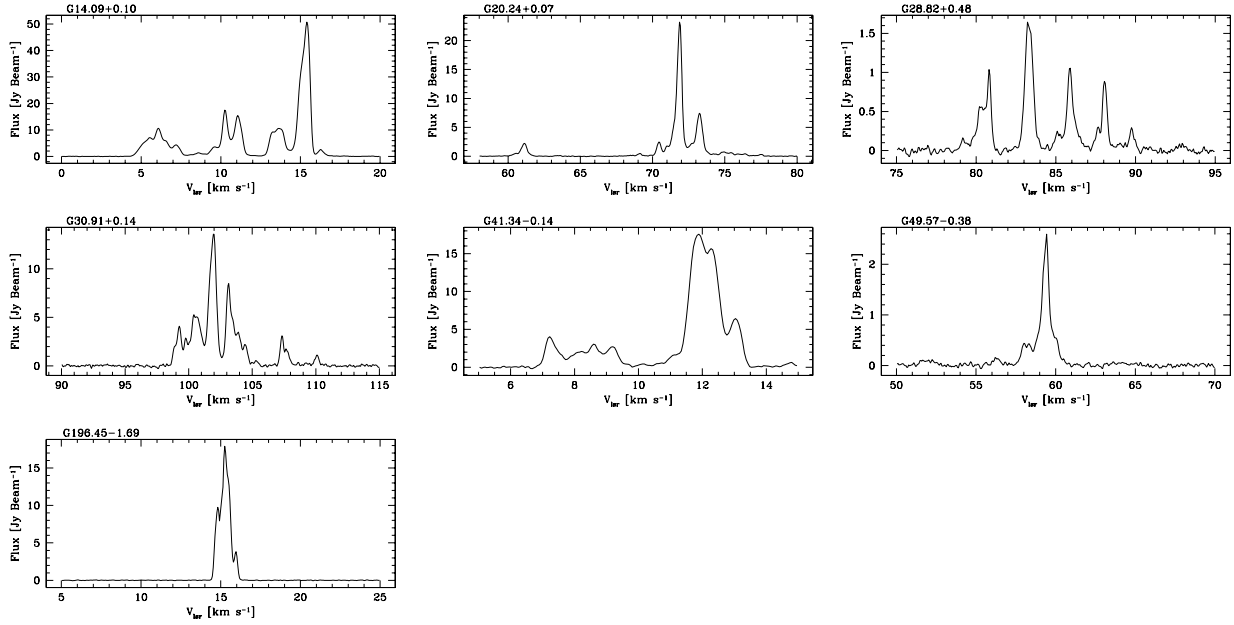


Fig. 6. Total intensity spectra of the sources in our sample observed with Effelsberg for which no significant Zeeman splitting was detected.

Table 2. Parkes observations.

Source	Other name	α_{J2000} (hh mm ss)	δ_{J2000} ($^{\circ}$ ' ")	V_{LSR} (km s $^{-1}$)	Peak flux (Jy beam $^{-1}$)	Int. flux Jy beam $^{-1}$ km s $^{-1}$
G06.78-0.27	IRAS 17589-2312	18 01 57.200	-23 12 37.00	26.9	63	191
G08.68-0.36	IRAS 18032-2137	18 06 23.500	-21 37 23.00	43.0	193	194
G09.62+0.20	IRAS 18032-2032	18 06 14.659	-20 31 31.57	1.0	6002	2769
G12.68-0.18	W33B	18 13 54.200	-18 01 44.00	52.0	527	1382
G12.90-0.26	IRAS 18117-1753, W33A	18 14 39.520	-17 52 00.00	39.0	328	378
G35.20-1.74	IRAS 18592+0108, W48	19 01 45.600	01 13 28.00	43.5	623	780
G49.49-0.39	IRAS 19213+1424	19 23 44.500	14 30 31.00	59.0	1045	879
G213.70-12.6	IRAS 06053-0622, MonR2	06 07 47.870	-06 22 57.00	12.0	499	264
G232.62+0.99	IRAS 07299-1651	07 32 09.790	-16 58 12.50	23.0	211	105
G263.25+0.52	IRAS 08470-4243	08 48 47.850	-42 54 28.00	13.0	82	72
G291.27-0.70	IRAS 11097-6102	11 11 53.370	-61 18 23.50	-30.0	78	109
G305.21+0.21	IRAS 13079-6218	13 11 14.400	-62 34 26.00	-38.0	517	464
G309.92+0.47	IRAS 13471-6120	13 50 41.850	-61 35 11.00	-60.0	1185	1371
G310.13+0.75	IRAS 13484-6100	13 51 54.200	-61 16 18.00	-56.0	80	103
G316.64-0.08	IRAS 14404-5942	14 44 18.430	-59 55 12.00	-20.0	132	242
G318.94-0.19		15 00 55.400	-58 58 53.50	-35.0	801	746
G322.16+0.64		15 18 34.300	-56 38 10.00	-63.0	376	768
G323.74-0.26	IRAS 15278-5620	15 31 45.410	-56 30 50.00	-51.0	3544	5674
G326.47+0.70	IRAS 15394-5358	15 43 18.000	-54 07 57.00	-38.1	150	155
G328.23-0.54	IRAS 15541-5349	15 57 58.280	-53 59 22.50	-44.9	1661	1295
G329.02-0.20	IRAS 15566-5304	16 00 33.300	-53 13 02.00	-37.5	156	305
G331.27-0.18	IRAS 16076-5134	16 11 26.560	-51 41 56.50	-78.1	111	277
G336.01-0.82	IRAS 16313-4840	16 35 09.300	-48 46 47.00	-45.0	105	218
G337.70-0.05	IRAS 16348-4654	16 38 29.620	-47 00 35.00	-54.6	218	297
G339.05-0.31	IRAS 16411-4604	16 44 49.090	-46 10 14.00	-111.6	168	153
G339.88-1.25	IRAS 16484-4603	16 52 04.670	-46 08 34.00	-39.0	1980	3408
G340.79-0.10	IRAS 16465-4437	16 50 17.000	-44 42 22.00	-107.0	175	328
G341.22-0.21	IRAS 16487-4423	16 52 17.900	-44 26 41.00	-38.0	196	356
G345.00-0.22	IRAS 17016-4124	17 05 10.900	-41 29 06.50	-22.0	119	283
G345.01+1.79	IRAS 16533-4009	16 56 47.560	-40 14 25.50	-18.0	334	705
G345.50+0.34	IRAS 17008-4040	17 04 22.890	-40 44 23.00	-18.0	369	945
G351.41+0.64	IRAS 17175-3544, NGC 6334F	17 20 53.370	-35 47 02.00	-10.0	3784	3096
G351.77-0.53	IRAS 17233-3606	17 26 42.560	-36 09 17.50	2.0	332	290
G354.61+0.47	IRAS 17269-3312	17 30 16.800	-33 14 13.00	-23.0	221	355

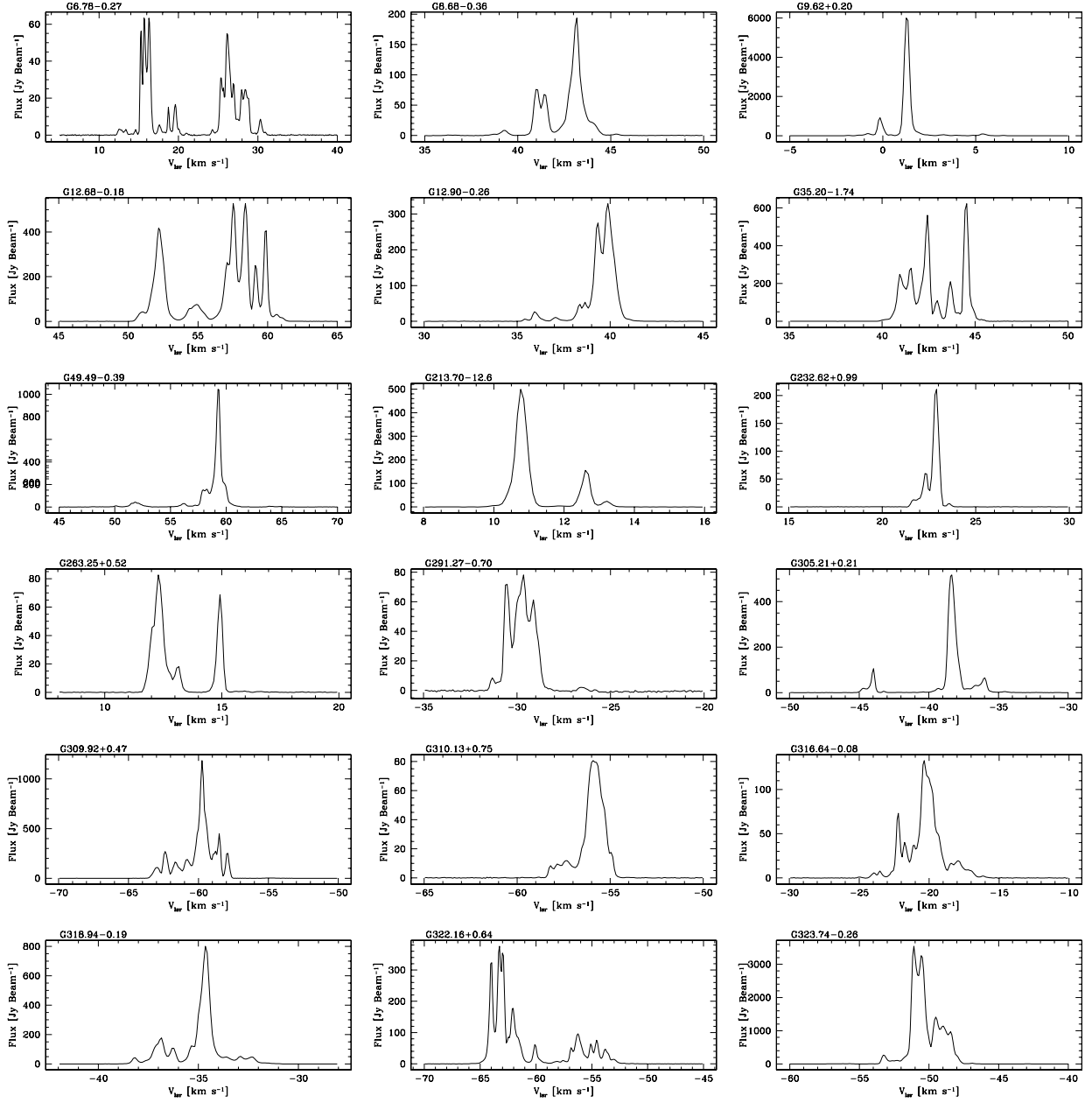


Fig. 7. Total intensity spectra of the sources in our sample observed with Parkes for which we were unable to determine the Zeeman splitting.

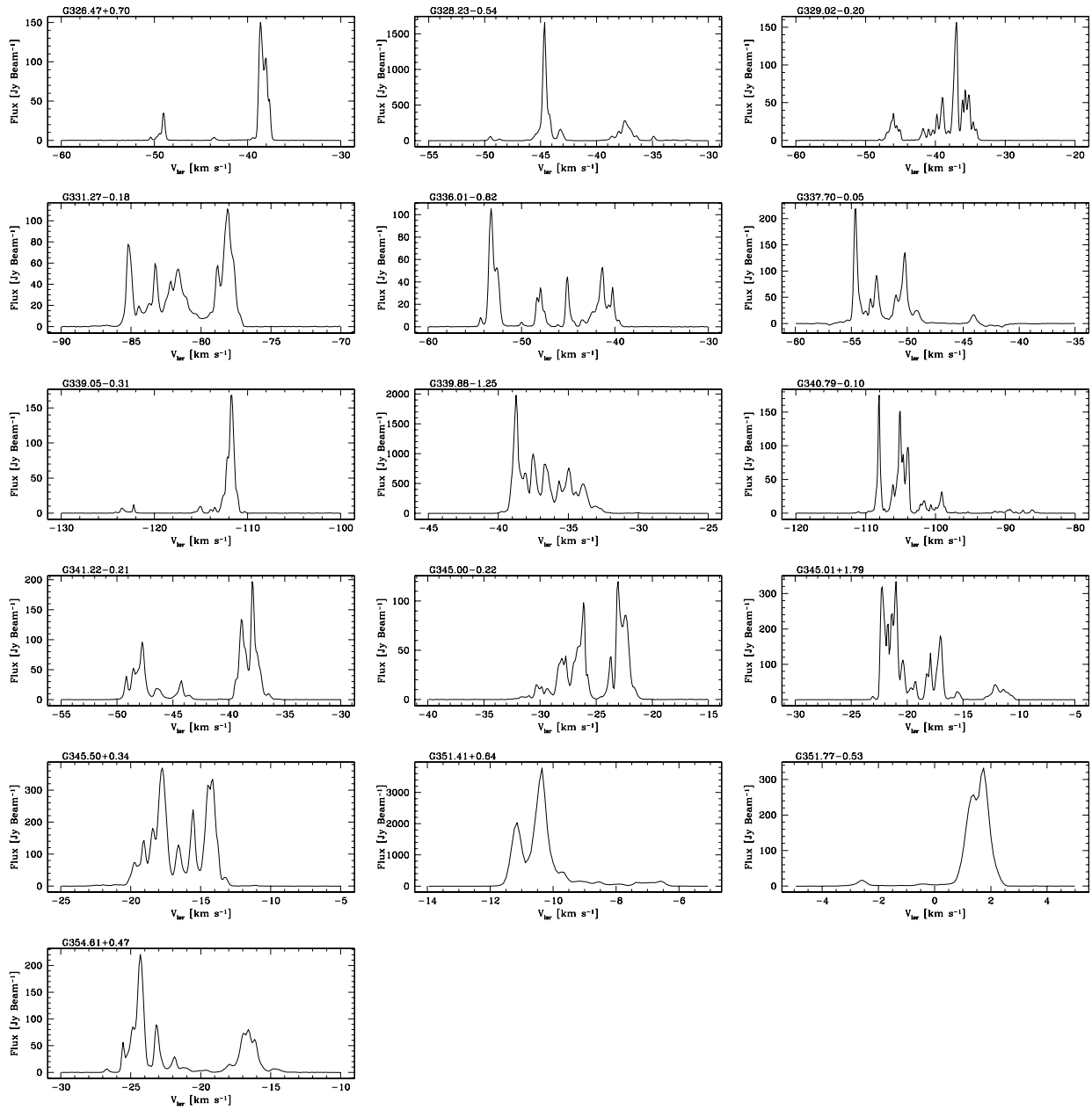


Fig. 7. continued.